EXTENDED PDF FORMAT
SPONSORED BY
usb
www.usbweb.com

Splitting of the 520-Kilometer Seismic Discontinuity and Chemical Heterogeneity in the Mantle

Ashima Saikia, *et al.*

Science **319**, 1515 (2008);
DOI: 10.1126/science.1152818

The following resources related to this article are available online at www.sciencemag.org (this information is current as of March 18, 2008):

Updated information and services, including high-resolution figures, can be found in the online version of this article at:
http://www.sciencemag.org/cgi/content/full/319/5869/1515

Supporting Online Material can be found at:
http://www.sciencemag.org/cgi/content/full/319/5869/1515/DC1

This article **cites 31 articles**, 3 of which can be accessed for free:
http://www.sciencemag.org/cgi/content/full/319/5869/1515#otherarticles

This article appears in the following **subject collections**:
Geochemistry, Geophysics
http://www.sciencemag.org/cgi/collection/geochem_phys

Information about obtaining **reprints** of this article or about obtaining **permission to reproduce this article** in whole or in part can be found at:
http://www.sciencemag.org/about/permissions.dtl

Downloaded from www.sciencemag.org on March 18, 2008

Science (print ISSN 0036-8075; online ISSN 1095-9203) is published weekly, except the last week in December, by the American Association for the Advancement of Science, 1200 New York Avenue NW, Washington, DC 20005. Copyright 2008 by the American Association for the Advancement of Science; all rights reserved. The title *Science* is a registered trademark of AAAS.

to be formed in different media, whereas the inner surface of the tube can be tuned for a targeted application by selecting a second type of constitutive block of appropriate characteristics and properties.

References and Notes

1. B. H. Zimm, W. H. Stockmayer, *J. Chem. Phys.* **17**, 1301 (1949).
2. V. Bloomfield, B. H. Zimm, *J. Chem. Phys.* **44**, 315 (1966).
3. R. Dulbecco, M. Vogt, *Proc. Natl. Acad. Sci. U.S.A.* **50**, 236 (1963).
4. J. C. T. Carlson *et al.*, *J. Am. Chem. Soc.* **128**, 7630 (2006).
5. A. Deffieux, R. Borsali, in *Macromolecular Engineering: Precise Synthesis, Materials Properties, Applications*, K. Matyjaszewski, Y. Gnanou, L. Leibler, Eds. (Wiley-VCH, Weinheim, Germany, vol. 2, 2007), pp. 875–908.
6. J. A. Semlyen, G. R. Walker, *Polymer* **10**, 597 (1969).
7. C. W. Bielawski, D. Benitz, R. H. Grubbs, *Science* **297**, 2041 (2002).
8. E. F. Cassassa, *J. Polym. Sci. A* **3**, 605 (1965).
9. B. Vollmert, J. X. Huang, *Makromol. Chem. Rapid Commun.* **2**, 467 (1981).
10. G. Hild, C. Strazielle, P. Rempp, *Eur. Polym. J.* **19**, 721 (1983).
11. J. Roovers, P. Toporowski, *Macromolecules* **16**, 843 (1983).
12. T. E. Hogen-Esch, *J. Polym. Sci. Polym. Chem.* **44**, 2139 (2006).
13. M. Schappacher, A. Deffieux, *Makromol. Chem. Rapid Commun.* **12**, 447 (1991).
14. Y. Tezuka, H. Oike, *J. Am. Chem. Soc.* **123**, 11570 (2001).
15. A. Deffieux, M. Schappacher, *Macromolecules* **32**, 1797 (1999).
16. G. Hadziioannou *et al.*, *Macromolecules* **20**, 493 (1987).
17. M. Schappacher, A. Deffieux, *Macromolecules* **33**, 7371 (2000).
18. M. Schappacher, Z. Muchtar, A. Deffieux, *Macromolecules* **34**, 7595 (2001).
19. P. Viville *et al.*, *Polymer* **45**, 1833 (2004).
20. M. Schappacher, C. Billaud, C. Paulo, A. Deffieux, *Macromol. Chem. Phys.* **200**, 2377 (1999).
21. Assignment of peaks and peak shoulders on the SEC of polymer brushes to dimer, linear, and cyclic structures (Fig. 2) was made on the basis of their radius of gyration measured by SLS with a online laser light scattering detector.
22. M. Schappacher, A. Deffieux, *Macromolecules* **38**, 4942 (2005).
23. S. S. Sheiko, M. Möller, *Chem. Rev.* **101**, 4099 (2001).
24. S. S. Sheiko, in *Advances in Polymer Science: New Developments in Polymer Analytics II* (Springer Berlin, Heidelberg, vol. 151, 2000), pp. 61–174.

Supporting Online Material

www.sciencemag.org/cgi/content/full/319/5869/1512/DC1
Materials and Methods
Figs. S1 to S3
References

6 December 2007; accepted 1 February 2008
10.1126/science.1153848

Splitting of the 520-Kilometer Seismic Discontinuity and Chemical Heterogeneity in the Mantle

Ashima Saikia,* Daniel J. Frost, David. C. Rubie

Seismic studies indicate that beneath some regions the 520-kilometer seismic discontinuity in Earth's mantle splits into two separate discontinuities (at ~500 kilometers and ~560 kilometers). The discontinuity near 500 kilometers is most likely caused by the $(Mg,Fe)_2SiO_4$ β-to-γ phase transformation. We show that the formation of $CaSiO_3$ perovskite from garnet can cause the deeper discontinuity, and by determining the temperature dependence for this reaction we demonstrate that regional variations in splitting of the discontinuity arise from variability in the calcium concentration of the mantle rather than from temperature changes. This discontinuity therefore is sensitive to large-scale chemical heterogeneity. Its occurrence and variability yield regional information on the fertility of the mantle or the proportion of recycled oceanic crust.

Recent regional seismic observations have identified multiple discontinuities near the depth of the 520-km discontinuity in the transition zone (*1*–*4*). Beneath some regions, this discontinuity splits into two discontinuities, one at a depth of about 500 km and the other near 560 km (*1*). The depth of these two discontinuities varies, implying that they are marking phase transitions that are responding to variations in composition between regions of the mantle or to varying temperature. The wadsleyite-to-ringwoodite (β-γ) transition is often implicated as the cause of the 520-km discontinuity (*5*). However, the exsolution of $CaSiO_3$ perovskite from majoritic garnet that also occurs at a similar depth could cause the observed higher pressure split in the 520-km discontinuity (*6*). This reaction is complex because majoritic garnet is a multicomponent solid solution. Existing data (*7*–*10*) are not sufficiently consistent for modeling how the reaction varies with respect to pressure, temperature, and mantle composition. We studied the exsolution of Ca perovskite in high-pressure and -temperature experiments in order to ascertain the depth interval over which the reaction occurs. We also estimated the jump in density and sound velocity expected for this reaction and used these data to explain regional occurrences of single and split 520-km discontinuities.

At mid-transition-zone pressures (17 GPa), garnet will contain all of the Ca in most plausible mantle chemical compositions and will have a substantial majorite component (i.e., $Mg_4Si_4O_{12}$), which results from the substitution of Si and Mg into the Al site at high pressure (*11*, *12*). The proportions of Ca and Al in transition-zone garnets will vary strongly between different rock types, being low in rocks of peridotite composition but much higher in rocks that are remnants of subducted oceanic crust, that is, with the composition of midocean ridge basalt (MORB). With increasing pressure, Ca perovskite exsolves from garnet as the solubility of $CaSiO_3$ in garnet decreases. We measured this solubility in multianvil experiments between 15 and 24 GPa at 1400° and 1600°C and as a function of the garnet majorite content (i.e., Al/Si ratio). Ca-free glass compositions on the join $(Mg,Fe)_4Si_4O_{12}$–$(Mg,Fe)_3Al_2Si_3O_{12}$ were mixed with presynthesized $CaSiO_3$ wollastonite in a 1:2 weight ratio to produce starting materials for multianvil experiments. These samples were loaded into rhenium capsules that contained four sample chambers (Fig. 1). Three samples with varying Al/Si ratios were loaded into each experiment, plus a $(Mg,Fe)_2SiO_4$ sample to calibrate the pressure. During the experiment, the glass and $CaSiO_3$ compositions crystallize rapidly to form garnet and perovskite, respectively, and $CaSiO_3$ dissolves into the garnet (*13*). The diffusion into the garnet is slow, and experiments must be equilibrated for at least 24 hours in order to reach equilibrium. A B_2O_3 flux was also added to speed up the reaction. Some experiments were reversed by first synthesizing Ca-bearing garnets and measuring their compositions after $CaSiO_3$ had subsequently exsolved at a particular pressure and temperature. After the experiments had been quenched, recovered samples were analyzed with an electron microprobe. During the experiments, the $(Mg,Fe)_2SiO_4$ olivine pressure calibrant crystallized to form coexisting high-pressure phases. The pressure could be determined because the high-pressure Mg_2SiO_4-Fe_2SiO_4 phase diagram consists of a series of two-phase divariant loops where the Fe/(Fe+Mg) ratios of coexisting phases are very sensitive to pressure. In this way, we calibrated accurately the pressure of Ca-perovksite formation relative to the pressure of phase transformations in the Mg_2SiO_4-Fe_2SiO_4 system (*13*–*15*).

Our data (Fig. 2) show that the solubility of $CaSiO_3$ in garnet in equilibrium with Ca perovskite decreases strongly with pressure, but it increases with the garnet Al/Si ratio at a given pressure, which can be seen by comparing results from the different starting compositions. At lower temperatures (1400°C), $CaSiO_3$ solubility in gar-

Bayerisches Geoinstitut, University of Bayreuth, D-95444 Bayreuth, Germany.

*To whom correspondence should be addressed. E-mail: ashima.saikia@uni-bayreuth.de

Downloaded from www.sciencemag.org on March 18, 2008

net also decreases. The exsolution can be described by the equation

$$\underset{\text{Garnet}}{Ca_3Al_2Si_3O_{12}} + \tfrac{3}{4}\underset{\text{Garnet}}{(Mg,Fe)_4Si_4O_{12}} = \underset{\text{Perovskite}}{3CaSiO_3} + \underset{\text{Garnet}}{(Mg,Fe)_3Al_2Si_3O_{12}} \quad (1)$$

We fit the experimental results to a thermodynamic model (*13*, *16*) for Eq. 1 that allows us to calculate the extent of exsolution for any bulk composition and reliably extrapolate the results to lower temperatures, where slow kinetics inhibit the achievement of equilibrium in experiments.

In the mid-transition zone, the Ca content of garnet in a fertile mantle peridotite composition (*18*) is constant with pressure up to about 19.7 GPa at 1600°C because garnet contains all the Ca in the bulk composition (Fig. 2A). Above this pressure, the garnet $CaSiO_3$ solubility limit is reached, and Ca perovskite exsolves. Because the Ca content of subducted oceanic crust (i.e., MORB) is higher, the garnet reaches saturation at lower pressures than in the peridotite composition (Fig. 2B), but the exsolution of Ca perovskite is offset somewhat because the MORB garnet has a higher Al content, which shifts $CaSiO_3$ saturation to higher pressures. The garnet becomes more Al-rich as $CaSiO_3$ exsolves and, for a MORB composition, the Al/Si ratio reaches its maximum, that is, that of pyrope (i.e., Al/Si = 2/3), above 23 GPa. At this point, if Ca perovskite is to continue to exsolve, an additional phase needs to form to accommodate the excess Al from the breakdown of garnet. In some previous experiments, a

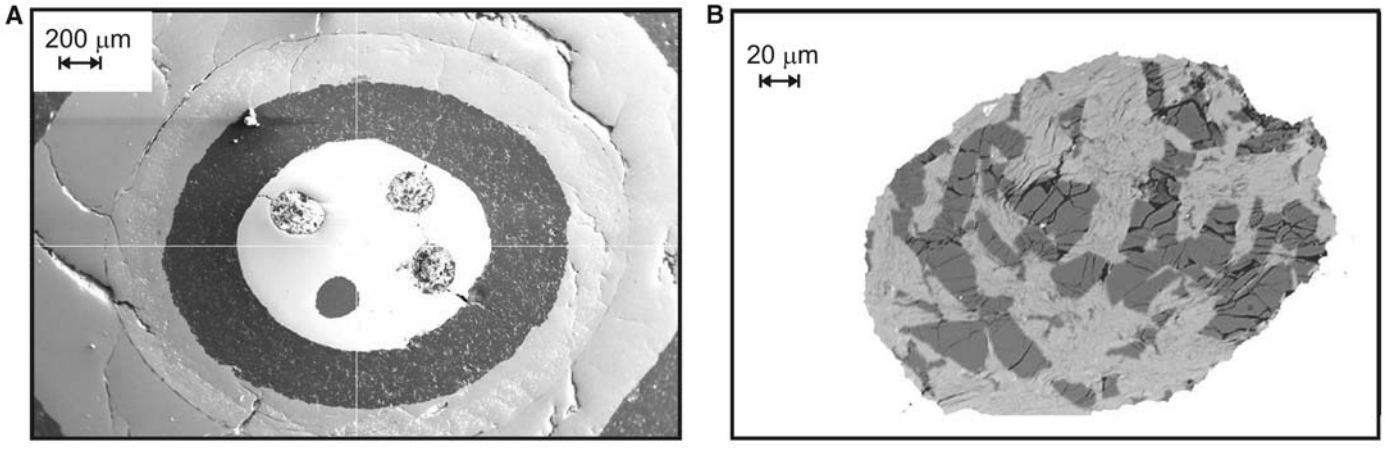

Fig. 1. Back-scattered electron images of sample capsules. (**A**) A radial section through the high-pressure assembly shows the outer pressure medium and furnace with an inner four-chamber Re capsule (white). Three sample chambers contain garnet and Ca-perovskite assemblages (which appear lighter), whereas the bottom left sample chamber contains a $(Mg,Fe)_2SiO_4$ pressure-calibrant sample (darker). (**B**) An enlargement of one of the sample chambers showing darker, angular garnet grains coexisting with lighter Ca perovskite. During the experiment, $CaSiO_3$ diffuses into the garnet until it becomes saturated in this component.

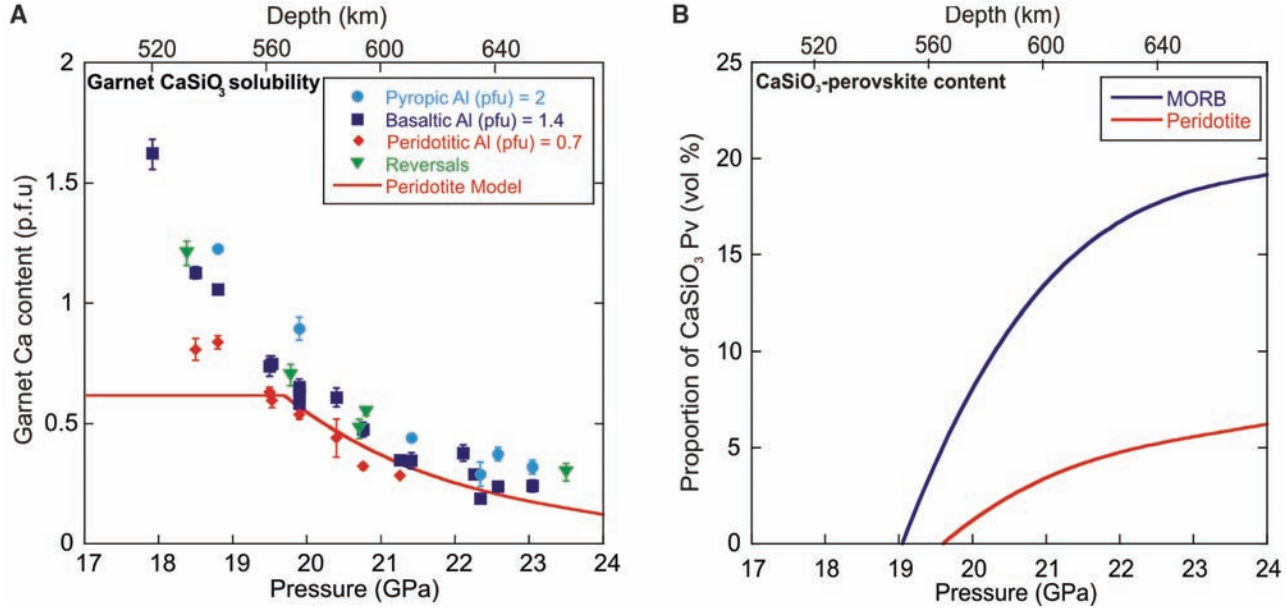

Fig. 2. (**A**) Experimental results showing the Ca content of garnet saturated with Ca perovskite as a function of pressure at 1600°C. Symbols refer to starting compositions, with different garnet majorite proportions labeled according to the rock types in which the garnets would be present. Al (pfu) refers to the Al content per garnet formula unit, that is, Al (pfu) = 2 refers to the formula $(Mg,Fe)_3Al_2SiO_{12}$ (i.e., pyropic). These Al contents only refer to those in the starting material because Al contents decrease as the garnets become $CaSiO_3$ saturated. The reversals were performed by using presynthesized Ca-bearing garnets. The curve shows the calculated Ca content of garnet for a peridotite composition (*18*). Below 19.7 GPa, the Ca content is constant with pressure because the garnet contains the entire Ca content of the rock, whereas in the experiments excess $CaSiO_3$ was always present. (**B**) The volumetric proportion of $CaSiO_3$ perovskite that forms as a function of pressure at 1600°C in rocks of peridotite and MORB compositions, respectively.

Downloaded from www.sciencemag.org on March 18, 2008

Na- and Al-rich phase [with the general formula $Na(Mg,Fe)_2Al_5SiO_{12}$] referred to as NAL has been observed that apparently serves this purpose [e.g., (*8*)]. The appearance of this Al-rich phase in a MORB composition is, therefore, directly coupled to the Ca perovskite–forming reaction and its influence on the Al content of garnet.

In Earth's mantle, the exsolution of Ca perovskite is inherently nonlinear because the activity of the garnet Ca component has an exponential relationship to pressure (*13*, *16*). Although Ca perovskite forms over an extensive depth range [about 60 km (*10*)], the transformation will appear sharper to seismic waves (*19*, *20*) because a substantial portion of the exsolution occurs initially over a relatively narrow depth interval, causing a moderately sharp change in density. Combining the experimental results with mineral physics data (*13*, *21*–*23*), we estimated the density and sound velocity changes that this exsolution reaction would produce (Fig. 3). For fertile peridotite at 1400°C, the β-γ transition produces a relatively strong discontinuity at 500 to 520 km, whereas the formation of Ca perovskite creates a break in slope at about 540 km, followed by a region with a higher velocity gradient, which curves back toward the ambient transition zone gradient over a depth interval of about 60 km. A similar situation occurs at 1600°C, but because the Clapeyron slope of the β-γ transition is steeper [~0.007 GPa K^{-1} (*24*)] than that of the Ca-perovskite reaction (~0.004 GPa K^{-1}), the two discontinuities merge at 540 to 560 km. Both discontinuities contribute to a generally steep gradient in seismic velocity in the lower part of the transition zone, which is a feature observed in most seismic reference models (*25*). For a MORB composition, no β-γ transition occurs, but because of the higher Ca content a strong discontinuity is caused as Ca perovskite forms.

Most observations of the 520-km discontinuity have been made with studies of long-period underside SS reflections (*1*, *5*, *26*), where the amplitude (i.e., the visibility of the reflected waves) depends on the S impedance contrast [$\Delta(\rho V_s)$]. The β-γ transition occurs over a depth interval of about 25 km with an estimated $\Delta(\rho V_s)$ of 3.6%. Although the seismically observable effective depth interval of the Ca-perovskite reaction is harder to determine and the reflectivity will vary with the frequency of the seismic waves (*19*, *20*), we can make a simple comparison by calculating $\Delta(\rho V_s)$ over the same depth interval as the β-γ transition, which gives an impedance contrast of about 1.5%. These impedance contrast estimates are in good agreement with those that have been proposed for the two discontinuities in regions where the 520 is split (*1*).

Many of the characteristics of splitting of the 520 could result from variations in mantle temperature. At ~1600°C, both transformations would merge into a single discontinuity, as observed in certain regions of Earth, whereas at lower temperatures (1400°C) two discontinuities would be observed. Although this may explain some of the observations, it is not completely consistent with the general behavior, which is that a discontinuity at about 520 to 530 km splits in some regions into a shallower (500 km) and a deeper (560 km) discontinuity (*1*). If this is a result of temperature variation alone, it would imply that the Clapeyron slope of the Ca-perovskite reaction is negative, whereas both the β-γ and Ca-perovskite reactions have positive slopes. In addition, at conditions where the two discontinuities merge, the single discontinuity should be substantially deeper than its typical depth of about 520 km (*27*). A more likely explanation is that, in many regions where only a single 520-km discontinuity is observed, the Ca-perovskite reaction is invisible because the Ca content of the mantle is too low. A low Ca content would result when a region has undergone partial melting near Earth's surface and thus became depleted in its fertile component. A strong 560 reflection, on the other hand, indicates the presence of fertile mantle or mantle that contains a substantial component of recycled MORB crust. The impedance contrast for the Ca-perovskite reaction in MORB is about 3%. Because the β-γ transition does not occur in a MORB composition, mantle enriched in subducted MORB crust would have a weak 500-km discontinuity but a much stronger reflection at about 560 km, which is consistent with observations (*1*).

One explanation for splitting of the 520 would be that it occurs in regions containing substantial amounts of subducted oceanic crust, which possesses higher Ca concentrations than normal mantle. This would be consistent with evidence for cooler-than-average mantle in these regions because the β-γ transition appears to be also slightly uplifted (*1*, *2*) as the 520 splits, although there are substantial uncertainties in absolute discontinuity depth estimates. If subducting slabs descend at a high angle directly into the lower mantle, such regions would not be expected to be globally extensive. However, the widespread splitting of 520 would be easily explained if subducted material is accumulating at the base of the transition zone (*28*, *29*), creating relatively low-temperature flat-lying regions rich in subducted crust. This hypothesis is supported by the geographical dis-

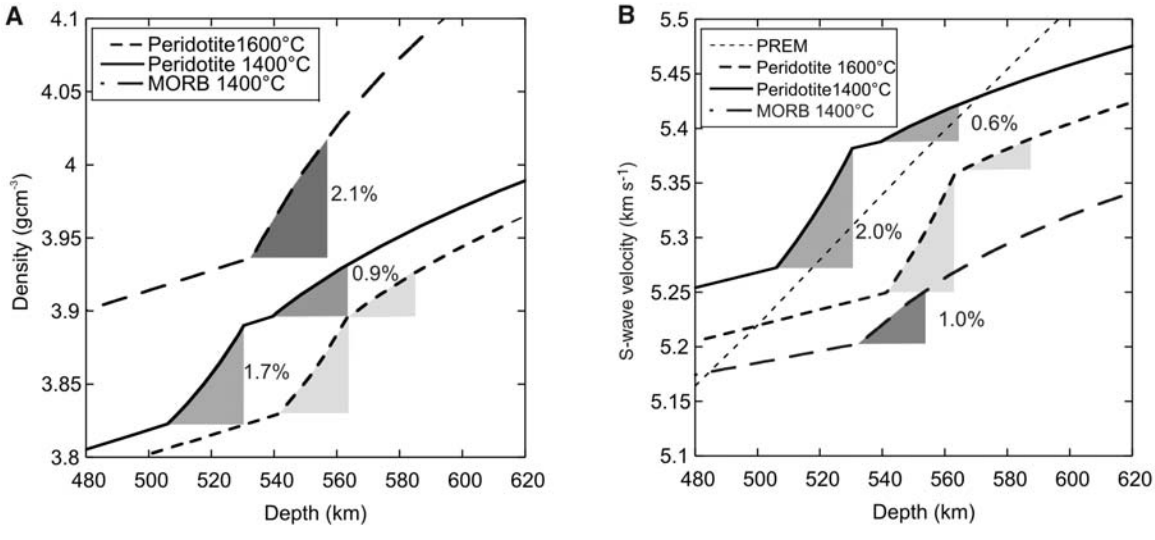

Fig. 3. (**A**) Density and (**B**) shear wave velocity estimated along isotherms for fertile peridotite (*18*) and MORB compositions as a function of depth, illustrating discontinuity structure in the region of 520 km. The phase proportions are calculated by using a thermodynamic model fitted to the experimental data in addition to auxiliary thermodynamic data for the $(Mg,Fe)_2SiO_4$ β-γ phase transformation (*13*, *14*). For the peridotite composition, two discontinuities (shaded) can be observed that result from the shallower β-to-γ and the deeper garnet exsolution of Ca-perovskite reactions. For the MORB composition, only the Ca-perovskite reaction occurs. Because the Ca-perovskite reaction is nonlinear and its seismically observable depth interval is difficult to assess, the shaded region is shown with the same depth interval as the β-γ transition for comparison. The percent density and S-wave velocity jumps resulting from both the β-γ and Ca-perovskite reactions are shown calculated over the shaded regions. Experimental uncertainties in discontinuity depths are about 10 km; density and velocity uncertainties are discussed in (*13*). Preliminary Reference Earth Model (PREM) S-wave velocity is shown for comparison.

Downloaded from www.sciencemag.org on March 18, 2008

tribution of split 520 observations, which in many instances occur beneath continental regions, such as North America and Eastern Asia (*1*–*4*), under which extensive subduction has taken place. Splitting beneath the Indian Ocean and Africa, on the other hand, may be caused by the presence of particularly fertile mantle.

References and Notes

1. A. Deuss, J. Woodhouse, *Science* **294**, 354 (2001).
2. H. J. Gilbert, A. F. Sheehan, K. G. Dueker, P. Molnar, *J. Geophys. Res.* **108**, 10.1029/2001JB001194 (2003).
3. A. Deuss, S. A. T. Redfern, K. Chambers, J. H. Woodhouse, *Science* **311**, 198 (2006).
4. M. van der Meijde, S. Van der Lee, D. Giardini, *Phys. Earth Planet. Inter.* **148**, 233 (2005).
5. P. M. Shearer, *Nature* **344**, 121 (1990).
6. J. J. Ita, L. Stixrude, *J. Geophys. Res.* **97**, 6849 (1992).
7. T. Gasparik, *Contrib. Mineral. Petrol.* **124**, 139 (1996).
8. K. Hirose, Y. Fei, *Geochim. Cosmochim. Acta* **66**, 2099 (2002).
9. K. D. Litasov, E. Ohtani, *Phys. Earth Planet. Inter.* **150**, 239 (2005).
10. Y. Nishihara, E. Takahashi, *Earth Planet. Sci. Lett.* **190**, 65 (2001).
11. G. R. Helffrich, B. J. Wood, *Nature* **412**, 501 (2001).
12. D. J. Weidner, Y. Wang, in *Earth's Deep Interior: Mineral Physics and Tomography From the Atomic to the Global Scale* [*Geophys. Monogr. 117 Am. Geophys. Union* (2000)], pp. 215–235.
13. Materials and methods are available on *Science* Online.
14. D. J. Frost, *Earth Planet. Sci. Lett.* **216**, 313 (2003).
15. K. Matsuzaka, M. Akaogi, T. Suzuki, T. Suda, *Phys. Chem. Miner.* **27**, 310 (2000).
16. At equilibrium the standard state free energy change $\Delta G^0_{P,T}$ for the reaction in Eq. 1 is related to the activities of the reacting components by the equation $\Delta G^0_{P,T} = -RT\ln K = -RT\ln\left[a^{Gt}_{Mg_3Al_2Si_3O_{12}}\right]\Big/\left[a^{Gt}_{Ca_3Al_2Si_3O_{12}}\right]\left[a^{Gt}_{Mg_4Si_4O_{12}}\right]^{\frac{3}{4}}$,

where R is the gas constant, K is the equilibrium constant, and the superscript Gt refers to garnet. The component activities are described by $a^{Gt}_{Mg_4Si_4O_{12}} = \gamma^{Gt}_{Mg_4Si_4O_{12}}(X^{oct}_{Maj})(X^{dodec}_{Mg})^3$,

$a^{Gt}_{Ca_3Al_2Si_3O_{12}} = \gamma^{Gt}_{Ca_3Al_2Si_3O_{12}}\left(1 - X^{oct}_{Maj}\right)\left(X^{dodec}_{Ca}\right)^3$ and

$a^{Gt}_{Mg_3Al_2Si_3O_{12}} = \gamma^{Gt}_{Mg_3Al_2Si_3O_{12}}\left(1 - X^{oct}_{Maj}\right)\left(X^{dodec}_{Mg}\right)^3$, where

γ is an activity coefficient, x is the component mole fraction, and oct and dodec refer to the octohedral and dodecahedral cation sites of garnet and majorite (Maj). After calculating activity coefficients for mixing on just the dodecahedral site with use of a symmetric ternary solution model (for Mg, Ca, and Fe), we fit calculated values for the $RT\ln K$ term to obtain the equation $\Delta G^0_{P,T} = 140763 + 26.773T - 12560P$. The ternary solution model uses the Margules interaction parameters $W_{FeMg} = 300$ (J/mol) and $W_{CaFe} = 2000$ (J/mol) taken from the literature (*17*), whereas the parameter $W_{MgCa} = 8000 + 300P$ (J/mol, P in GPa) is refined by using the experimental data (*13*). Trial refinements showed no improvement to the fit of the data when nonideal mixing on the garnet octahedral site was included or when a reciprocal solution model was used.
17. H. St. C. O'Neill, B. J. Wood, *Contrib. Mineral. Petrol.* **70**, 59 (1979).
18. W. F. McDonough, S.-s. Sun, *Chem. Geol.* **120**, 223 (1995).
19. G. R. Helffrich, B. J. Wood, *Geophys. J. Int.* **126**, F7 (1996).
20. L. Stixrude, *J. Geophys. Res.* **102**, 14835 (1997).
21. L. Li *et al.*, *Phys. Earth Planet. Inter.* **155**, 249 (2006).
22. S. V. Sinogeikin, J. D. Bass, *Geophys. Res. Lett.* **28**, 4335 (2001).
23. S. V. Sinogeikin, J. D. Bass, *Geophys. Res. Lett.* **29**, 10.1029/2001GL013937 (2002).
24. A. Suzuki *et al.*, *Geophys. Res. Lett.* **27**, 803 (2000).
25. A. M. Dziewonski, D. L. Anderson, *Phys. Earth Planet. Inter.* **25**, 297 (1981).
26. P. M. Shearer, *J. Geophys. Res.* **101**, 3053 (1996).
27. M. P. Flanagan, P. M. Shearer, *J. Geophys. Res.* **103**, 2673 (1998).
28. U. R. Christensen, *J. Geophys. Res.* **102**, 22435 (1997).
29. H. Kárason, R. D. Van der Hilst, in *The History and Dynamics of Global Plate Motion* (*Geophys. Monogr. 121 Am. Geophys. Union* (2000)], pp. 277–288.

30. We thank D. Dolejš and S. Jacobsen for numerous useful discussions. A.S. was funded through the Elitenetzwerk Bavaria, International Graduate School on "Structure, Reactivity and Properties of Oxide Materials."

Supporting Online Material

www.sciencemag.org/cgi/content/full/319/5869/1515/DC1
Materials and Methods
Tables S1 to S4

9 November 2007; accepted 24 January 2008
10.1126/science.1152818

The Chlorine Isotope Composition of Earth's Mantle

M. Bonifacie,[1,2] N. Jendrzejewski,[1] P. Agrinier,[1] E. Humler,[3,4] M. Coleman,[5,6] M. Javoy[1]

Chlorine stable isotope compositions (δ^{37}Cl) of 22 mid-ocean ridge basalts (MORBs) correlate with Cl content. The high-δ^{37}Cl, Cl-rich basalts are highly contaminated by Cl-rich materials (seawater, brines, or altered rocks). The low-δ^{37}Cl, Cl-poor basalts approach the composition of uncontaminated, mantle-derived magmas. Thus, most or all oceanic lavas are contaminated to some extent during their emplacement. MORB-source mantle has δ^{37}Cl ≤ -1.6 per mil (‰), which is significantly lower than that of surface reservoirs (~ 0‰). This isotopic difference between the surface and deep Earth results from net Cl isotopic fractionation (associated with removal of Cl from the mantle and its return by subduction over Earth history) and/or the addition (to external reservoirs) of a late volatile supply that is ^{37}Cl-enriched.

Chloride is the major anion in most geological fluids. Chlorine is volatile, incompatible during silicate melting, and water soluble. For these reasons, geological processes—including partial melting, magma degassing, hydrothermal activity, and weathering—have concentrated Cl at the surface, particularly in the ocean, evaporites, and crustal brines. Considering only the MORB-source mantle and surface reservoirs, we can estimate that the former, with 1 to 8 parts per million (ppm) of Cl (*1*–*3*), contributes a maximum of ~ 20% to the Cl budget and perhaps much less, given the difficulty in obtaining a complete inventory of crustal brines. Earth's Cl budget may thus differ from that of most other abundant and geochemically important volatiles (e.g., H_2O, CO_2).

There are several first-order questions about Cl in Earth: What early solar system processes determined Earth's initial Cl budget? How, and when, was most of Earth's Cl extracted from the mantle? How much Cl is returned to the mantle by subduction? Is the extraction of Cl from, and its return to, the mantle in steady state? If not, what can we learn about the history of Earth's volatile cycles by reconstructing secular changes in the Cl budgets of the mantle and/or surface? These questions can be addressed by determining δ^{37}Cl (*4*) of the various reservoirs in that budget and isotopic fractionations associated with exchanges between those reservoirs. Surface reservoirs (mostly oceans, brines, and evaporites) are known to have a collective mean δ^{37}Cl of 0.0 ± 0.5‰ (*5*–*8*). However, it is more difficult to measure the δ^{37}Cl of pristine mantle rocks and mantle-derived magmas because both are generally poor in Cl (*1*–*3*), which is usually present in insoluble form. Here, we present measurements of 22 MORBs that define the mantle composition to lower δ^{37}Cl values than previously assumed (*9*, *10*) and use these results to examine the origin and history of Earth's volatiles.

The first attempt to define the Cl isotope composition of the mantle used thermal ionization mass spectrometry (TIMS) to analyze three MORB samples (*9*), yielding an average mantle value of +4.7‰. Sharp *et al.* (*10*) recently used gas-source mass spectrometry to determine a mantle δ^{37}Cl value of –0.1 ± 0.4‰, which was derived from the average of 11 MORB samples, two kimberlites, and three carbonatites. They suggested δ^{37}Cl homogeneity near the seawater value (0‰) for mantle and surface reservoirs over Earth's history (*10*). This implies that neither removal of Cl from the mantle nor its

[1]Equipe de Physico-Chimie des Fluides, Géologiques, Institut de Physique du Globe de Paris (IPGP) and Université Paris, Diderot (UPD), CNRS-INSU–Unité Mixte de Recherche (UMR) 7154, 75251 Paris Cedex 05, France. [2]Division of Geological and Planetary Sciences, California Institute of Technology (CalTech), Pasadena, CA 91125, USA. [3]Equipe de Géosciences Marines, IPGP, CNRS-INSU-UMR 7154, 75251 Paris Cedex 05, France. [4]Laboratoire de Planétologie et Géodynamique, Université de Nantes, CNRS UMR 6112, 44322 Nantes Cedex 3, France. [5]School of Human and Environmental Sciences, University of Reading, RG6 6AB, UK. [6]Jet Propulsion Laboratory, CalTech, Pasadena, CA 91109, USA.

*To whom correspondence should be addressed. E-mail: bonifaci@gps.caltech.edu

Downloaded from www.sciencemag.org on March 18, 2008